# Structural and Morphological Characteristics of Perovskite $CaTiO_3$ Derived from Tebalan Seashells for the Development of VOC Gas Sensing Materials

Roihatur Rohmah [a], Midya Yulia Amreta,[b,*] Nur Mahmudah [c] and Pelangi Eka Yuwita [d,*]

** Corresponding authors: midyaamreta2@gmail.com, pelangi@unugiri.ac.id*

*DOI: 10.15376/biores.21.2.3609-3621*

## GRAPHICAL ABSTRACT

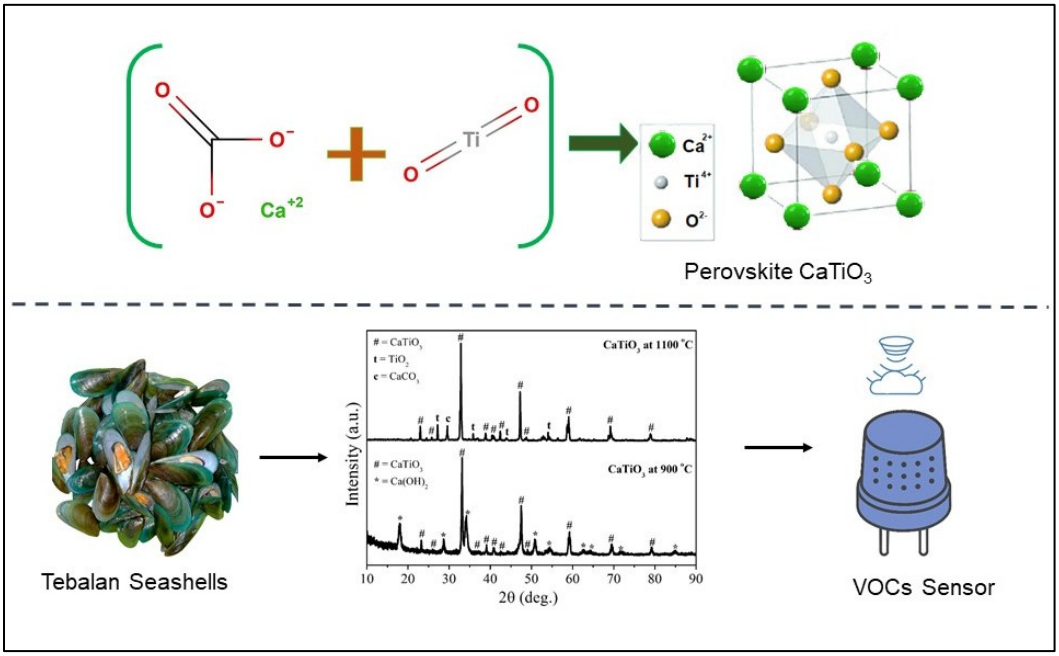

# Structural and Morphological Characteristics of Perovskite $CaTiO_3$ Derived from Tebalan Seashells for the Development of VOC Gas Sensing Materials

Roihatur Rohmah [a], Midya Yulia Amreta,[b,*] Nur Mahmudah [c] and Pelangi Eka Yuwita [d,*]

Perovskite $CaTiO_3$ mineral was synthesized from natural materials of Tebalan seashells and their structural and morphological characteristics were explored. The solids were calcined at temperatures of 900 °C and 1100 °C. The analysis by X-ray diffraction (XRD) demonstrated that the dominant phase of $CaTiO_3$ exhibited an orthorhombic structure, characterized by lattice parameters a = 5.388 Å, b = 5.446 Å, and c = 7.651 Å, at a temperature of 1100°C. This observation signifies an enhancement in crystallinity and an augmentation in phase purity. Scanning electron microscopy (SEM) showed that the morphology was homogeneous, with uniform grains and increased density at high temperatures. This morphology is indicative of the material's potential for use in VOC gas sensor applications, based on the observed regularity and density of the surface structure. It is hypothesized that the intrinsic porosity of shell-derived $CaTiO_3$, when coupled with the hierarchical porous architecture of lignocellulosic biomass, can synergistically enhance VOC adsorption and mass transfer, thereby significantly improving sensor sensitivity and detection performance. This outcome validates its promise as an eco-friendly and cost-effective VOC gas sensor material.

*DOI: 10.15376/biores.21.2.3609-3621*

*Keywords: Calcination temperature; Natural-derived minerals; Perovskite $CaTiO_3$; Tebalan seashells; VOCs gas sensor*

*Contact information: a: Department of Computer Systems, Faculty of Sains and Technology, Universitas Nahdlatul Ulama Sunan Giri, Indonesia; b: Department of Madrasah Ibtidaiyah Teacher Education, Faculty of Tarbiyah, Universitas Nahdlatul Ulama Sunan Giri; c: Department of Statistics, Faculty of Sains and Technology, Universitas Nahdlatul Ulama Sunan Giri, Indonesia; d: Department of Mechanical Engineering, Faculty of Sains and Technology, Universitas Nahdlatul Ulama Sunan Giri, Indonesia;*
** Corresponding author: pelangi@unugiri.ac.id*

## INTRODUCTION

The increase in the concentration of volatile organic compounds (VOCs) in urban environments is attributable to two key factors: climate change and the degradation of air quality caused by rapid urbanization (Zhou *et al.* 2023). The carbon-based VOCs such as toluene, formaldehyde, methanol, and ethanol are characterized by their high volatility and significant toxic and carcinogenic potential (David and Niculescu 2021). The long-term inhalation of VOCs has been demonstrated in scientific literature to be a contributing factor to the development of respiratory issues, ocular irritation, and dermal inflammation. Moreover, there is an increased probability of developing chronic diseases, including, but not limited to carcinogenesis, in cases of long-term exposure (Dehghani *et al*. 2024). Consequently, the development of rapid, sensitive, and selective detection systems against

VOCs is imperative in the present day. The necessity for such capabilities arises from the importance of accurate detection in maintaining environmental safety and protecting public health from exposure to harmful gases.

Conventional gas sensors, particularly Metal Oxide Semiconductor (MOS) based sensors, are extensively utilized for the detection of VOCs. However, it should be noted that these sensors generally require an operating temperature of 200 to 500°C to achieve adequate levels of sensitivity and selectivity (Wawrzyniak 2023). Furthermore, the ability to withstand prolonged exposure to moisture and material degradation poses a significant challenge. Sensor materials must be selected that are capable of operating at ambient temperature and demonstrating consistent performance, a consideration that assumes particular significance in the context of portable applications and real-time air monitoring systems.

Wood-based materials are widely used for VOCs control because they are abundant, renewable, and environmentally friendly. The natural pore structure of wood supports the diffusion of gases as well as the absorption of VOC molecules through hydrogen bonds and Van der Waals interactions. Carbonization and activation processes increase surface area and adsorption capacity (Adamová *et al*. 2020; Zhang *et al*. 2022; Rong *et al*. 2023). Biochar and wood-based activated carbon effectively absorb formaldehyde, toluene, and benzene due to oxygen and microporous functional groups (Zouari *et al*. 2023; Zhang *et al*. 2024). However, physical adsorption mechanisms with no electronic activity limit the ability of direct detection of the gas. In addition, the thermal and chemical stability of wood is low at high temperatures (Hill *et al*. 2021). Therefore, naturally occurring calcium-based minerals such as perovskite $CaTiO_3$ offer a more stable and sensitive alternative for VOCs detection.

In recent years, perovskite materials, encompassing perovskite halides and perovskite oxides, have emerged as significant contenders for use in VOC sensors (Ray and Basu 2023). These materials have been demonstrated to exhibit advantageous properties concerning plastic crystal lattice, efficient charge transfer, and their amenability to production through solution-based methods, which are presumed to engender reduced manufacturing expenses. The research by Singh *et al*. (2024) covers the influence of factors such as composition differences, morphology, crystal flaws, and surface structures on the conduct of perovskite-based VOC sensors (Singh *et al*. 2024).

One of the most innovative aspects of materials research is the use of local resources as precursors to functional materials. For example, Tebalan seashell waste (a type of shellfish typically found at Tuban Beach) is rich in calcium carbonate ($CaCO_3$). Calcium carbonate can be converted to calcium oxide (CaO), which can then be used as a component in the synthesis of perovskite oxides or as a support material (substrate or filler). Using local biomaterials in this way not only reduces the cost and environmental impact of producing materials, but it also supports the circular economy and adds a local dimension to scientific research.

Recent studies have also demonstrated that perovskite oxides and perovskite-modified materials can detect VOCs with low detection limits and operate at room temperature or moderate temperatures (Tan *et al.* 2025). Methylammonium lead iodide ($MAPbI_3$) films, for example, exhibit a sensitive response to a wide range of polar and non-polar VOCs at room temperature (Hossain and Takshi 2021). Furthermore, studies on perovskite oxide $ABO_2$ materials combined with heterostructures and doping showed significant increases in conductivity when exposed to VOC gases (such as acetone), even at lower temperatures than traditional sensors (Wu *et al*. 2023).

As previously discussed, there remains a paucity of research on the fabrication of gas sensor materials from perovskites that are derived from local biomineral sources. Specifically, the utilization of Tebalan seashells as a source for calcium oxide (CaO) in the synthesis of perovskite oxides has received scant attention as a potential material for the detection of VOCs. Furthermore, there is a paucity of research that has examined the way the crystal structure, surface geometry, and chemical composition of perovskites derived from such natural materials impact their capacity to absorb and react with gases. The objective of this study was to address these knowledge gaps by synthesizing and examining perovskite materials using CaO derived from Tebalan shells. The primary focus of this study was to examine and analyze the structural, morphological, and electronic properties of the samples that are deemed to be significant for the purpose of gas sensing. This research endeavor sought to examine the potential of the material as a prospective sensor candidate, whilst eschewing any involvement in the manufacturing process or the evaluation of the device itself. The findings are expected to contribute to the advancement of material physics by demonstrating the viability of sustainable biomineral sources as eco-friendly materials for perovskite synthesis and by providing a robust scientific foundation for future research in gas sensor materials.

## EXPERIMENTAL

### Materials

The calcium carbonate ($CaCO_3$) employed in this product was sourced from the shells of Tebalan, which were harvested from the coast of Tuban in Indonesia. Titanium dioxide ($TiO_2$, analytical grade, 99% purity, Merck, Darmstadt, Germany) was utilized as the titanium source. Ethanol ($C_2H_5OH$, analytical grade, purity 99.8%, Merck, Darmstadt, Germany) was utilized as the dispersing medium during the mixing process.

### Manufacture of Calcium Carbonate

The manufacturing process of calcium titanate, represented by the formula $CaTiO_3$, involves a perovskite structure. The initial step involves the preparation of $CaCO_3$, which was obtained from Tebalan seashells powder.

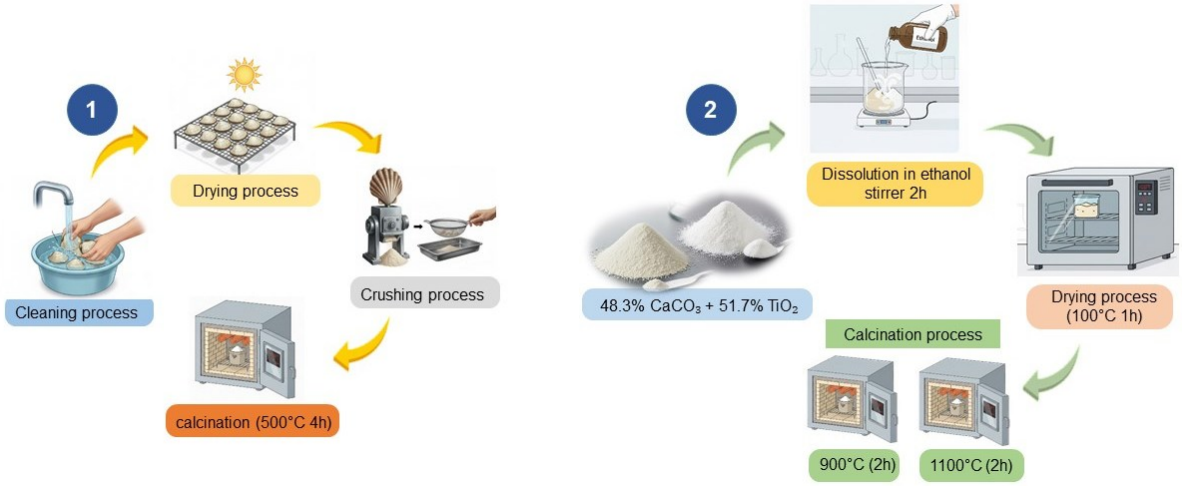


**Fig. 1.** Illustration of Synthesis $CaCO_3$ and $CaTiO_3$

The seashells were meticulously washed in running water and then dried in the sun. Subsequently, the seashells were subjected to a crushing process, which resulted in the production of a finer size. This material was then sifted through a 200-mesh sieve, a process that serves to separate the small and uniform particles. In addition, the seashells powder underwent calcination at a temperature of 500 °C for a duration of 4 h (Rohmah *et al*. 2024). This process was undertaken to eliminate impurities and volatile components from the precursor, thereby ensuring more homogeneous reaction in subsequent calcination stages. This approach also mitigated the likelihood of undesirable reactions, the formation of secondary phases, and grain size growth that is challenging to regulate (Zhao *et al.* 2021). The process is illustrated Fig. 1.

## Production of Calcium Titanate

The synthesis of calcium titanate ($CaTiO_3$) started with the calcination process of $CaCO_3$ from Tebalan seashells and titanium dioxide ($TiO_2$), which possesses a composition of 48.3% $CaCO_3$ and 51.7% $TiO_2$. The experiment involved the suspension of $CaCO_3$ powder and $TiO_2$ powder in ethanol, with the mixture being stirred using a magnetic stirrer for a duration of 2 h at room temperature. The function of ethanol was to mix the ingredients well when wet, making everything mix more evenly and helping to prevent clumping. This helped the particles to contact each other better and ensured a uniform and good quality final product (Arf *et al.* 2024). The slurry underwent a drying process in an oven at a temperature of 100 °C for a duration of one hour. The mixture of powders was then calcinated in furnaces at temperatures of 900 and 1100 °C for a duration of 2 h. This process was carried out at a rate of 10 °C/min to yield a fine powder of calcium titanate. The process illustration shown in Fig. 1.

## Testing

Following the synthesis process of Tebalan seashells into calcium titanate ($CaTiO_3$), a series of tests were conducted to demonstrate that $CaTiO_3$ from thick shells can be utilized as a constituent for the fabrication of VOC gas sensors. The present study reports the findings of physical testing conducted for the purpose of microstructure characterization of perovskite $CaTiO_3$.

## X-Ray Diffraction

Material characterization was undertaken using Type X-Pert3 Powder X-ray diffractometer, to determine the characteristics of the crystal structure of the powder materials used in the manufacture of perovskite polymer composite sensor $CaTiO_3$. XRD testing was conducted on $CaCO_3$ samples following calcination and on $CaTiO_3$ samples after calcination. The XRD testing was carried out at scan speed / duration time of 10°/minute, step width of 0.02°, scan axis of $2\theta/\theta$, and scan range of 5° to 90°.

## Scanning Electron Microscope-Energy Dispersive X-ray

The Scanning Electron Microscope-Energy Dispersive X-ray (SEM-EDX) technique was utilized to ascertain the morphology of the surface and to demonstrate the elements present in the perovskite material, $CaTiO_3$. The SEM-EDX assay utilized magnifications of 10,000 and 21,000 K on $CaTiO_3$ perovskite samples.

## RESULTS AND DISCUSSION

### Crystal Structure of Perovskite

The results of the data analysis of the diffraction patterns, conducted with the software program Match!, revealed that there were two phases for the 900 °C samples and three phases for the 1100 °C samples. These results are apparent from Table 1 and Fig. 2.

**Table 1.** Number of Phases Formed, 2 Specific Theta and Position of the Hkl Plan

| Phase Codes | 2θ (°) | | Peak Position of Hkl | |
|---|---|---|---|---|
| | 900 °C | 1100 °C | 900 °C | 1100 °C |
| # [$CaTiO_3$] | 23.23 | 22.98 | [002] | [110] |
| | 33.11 | 25.77 | [112] | [111] |
| | 39.06 | 32.86 | [211] | [112] |
| | 40.86 | 36.74 | [022] | [021] |
| | 42.64 | 38.86 | [202] | [210] |
| | 44.28 | 40.71 | [113] | [121] |
| | 47.51 | 42.41 | [122] | [103] |
| | 49.08 | 43.92 | [220] | [211] |
| | 59.20 | 47.56 | [124] | [022] |
| | 69.50 | 52.88 | [402] | [004] |
| | 71.93 | 54.33 | [332] | [123] |
| | 79.19 | 58.76 | [431] | [301] |
| | 84.43 | 59.06 | [433] | [130] |
| * [$Ca(OH)_2$] | 17.96 | | [001] | |
| | 28.68 | | [100] | |
| | 34.11 | | [101] | |
| | 50.85 | | [003] | |
| | 54.38 | | [200] | |
| | 59.20 | | [112] | |
| | 62.55 | | [202] | |
| | 64.15 | | [004] | |
| | 71.93 | | [113] | |
| | 79.19 | | [104] | |
| | 84.43 | | [300] | |
| t [$TiO_2$] | | 27.19 | | [110] |
| | | 35.83 | | [101] |
| | | 43.92 | | [201] |
| | | 54.33 | | [211] |
| | | 56.4 | | [220] |
| c [$CaCO_3$] | | 22.98 | | [102] |
| | | 29.57 | | [104] |
| | | 35.83 | | [110] |
| | | 47.56 | | [204] |
| | | 56.4 | | [211] |

The results of the XRD data of the synthesized sample using the software Match! demonstrated a highly significant correlation between the diffraction pattern of the sample and the reference data. The main peaks of diffraction that appeared at $2\theta$ = 23.3°, 32.8°, 40°, 47.2°, and 58.9° were successfully identified and matched with a typical crystal field (hkl) $CaTiO_3$, namely (110), (121), (202), (220), and (312), according to reference data COD 9002801 and COD 9006173.

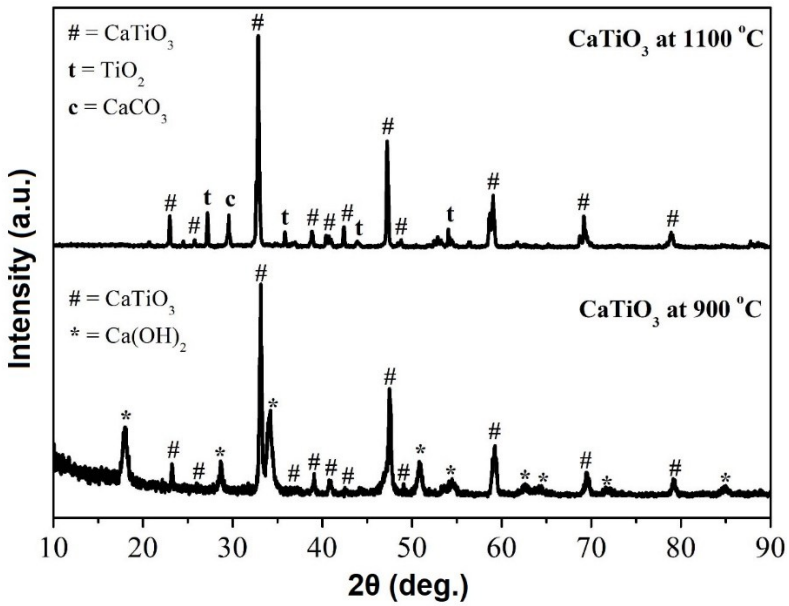


**Fig. 2.** XRD pattern calculation examples at 900 °C and 1100 °C

The similarity of the peak position, relative intensity, and sharp peak shape indicates that $CaTiO_3$ was the main phase with a high level of crystallinity. This finding serves to confirm that the solid reaction between the precursors $CaCO_3$ and $TiO_2$ had taken place perfectly at a temperature of 1100 °C, resulting in a stable orthorhombic perovskite structure.

In addition to the major phase $CaTiO_3$, the matching results also indicated the presence of several minor peaks corresponding to fields (101) and (200) of $TiO_2$ (rutile) with reference COD 1530150, as well as weak peaks at about $2\theta$ = 29.4° and 39.4° identified as fields (104) and (113) of $CaCO_3$ (calcite) with reference COD 7020139. The presence of these weak peaks is indicative of residual reactants or by-products resulting from the absorption of $CO_2$ during the cooling process. However, these peaks did not significantly influence the primary structure of the material. Its defining characteristic was the presence of known weight percentages of the $TiO_2$ and $CaCO_3$ phases, at only 10% and 9%, respectively (Table 2).

The results of the Rietveld refinement of the XRD data are presented in Table 2. The analysis demonstrated that $CaTiO_3$ (calcium titanate) was formed as the predominant phase at calcination temperatures of 900 and 1100 °C, accompanied by minor phases such as $Ca(OH)_2$, $TiO_2$, and $CaCO_3$, which appeared to be dependent on the synthesis temperature. It has been established that, at a temperature of 900 °C, the diffraction pattern was principally indexed in the orthorhombic perovskite phase of $CaTiO_3$ (Pbnm Space Group). In this phase, the lattice parameters were determined to be a = 5.388 Å, b = 5.432 Å, and c = 7.639 Å, with a cell volume of 223.567 $Å^3$. The minor phase $Ca(OH)_2$, with lattice parameters a = b = 3.589 Å and c = 4.912 Å (cell volume 54,808 $Å^3$), indicates the presence of a partial hydroxylation process in elemental calcium. This finding suggests that the solid reaction had not yet occurred fully at this temperature. The low density (2.244 $g/cm^3$) and relatively high R-Bragg (6.16) also support this conclusion. Furthermore, it was established that the weight percentage for 900°C was precisely 52.9% within the $CaTiO_3$ phase fraction. This indicates low crystallinity and structural irregularities at 900 °C.

**Table 2.** Results of the Refinement of the Crystal Diffraction Patterns in Samples Using Rietica

| Components | Structures | | | | |
|---|---|---|---|---|---|
| | 900 °C | | 1100 °C | | |
| | $CaTiO_3$ | $Ca(OH)_2$ | $CaTiO_3$ | $TiO_2$ | $CaCO_3$ |
| Lattice Parameter (Å) | a=5.388<br>b=5.432<br>c=7.639 | a=3.589<br>b=3.589<br>c=4.912 | a=5.388<br>b=5.446<br>c=7.651 | a=4.598<br>b=4.598<br>c=2.961 | a=5.071<br>b=5.071<br>c=16.411 |
| Cell Volume (Å³) | 223.567 ± 0.0712 | 54.808 ± 0.0251 | 224.547 ± 0.0293 | 62.623 ± 0.0151 | 365.511 ± 0.2215 |
| Density (g/cm³) | 4.038 | 2.244 | 4.021 | 4.235 | 2.727 |
| GoF | 1.29 | | | 2.566 | |
| R-Bragg | 4.01 | 6.16 | 3.71 | 2.41 | 14.01 |
| Weight Percentage (wt%) | 52.9 | 47,1 | 79.98 | 10.03 | 9.99 |

It was demonstrated that an elevation in calcination temperature to 1100 °C resulted in a substantial enhancement in crystallinity. It can thus be deduced that the percentage of weight was now 79.98%. The structure of $CaTiO_3$ underwent a slight lattice expansion with parameters a = 5.388 Å, b = 5.446 Å, and c = 7.651 Å, and the cell volume increased to 224.547 $Å^3$. This change is attributable to thermal relaxation and an increase in the order of atoms within the perovskite lattice. The R-Bragg value of 3.71 and the GoF of 2.566 indicate good refinement quality, *i.e.*, that the difference between the experimental and the simulated diffraction patterns was negligible (Toso *et al*. 2023). It is evident that minor alterations in the lattice parameters, as evidenced by the comparison with the standard $CaTiO_3$ parameters, were indicative of lattice relaxation resulting from heating at elevated temperatures (Zhu *et al*. 2023). This phenomenon makes it possible to generate oxygen vacancies in the crystal structure (Wang *et al*. 2022). This vacuum has been shown to play an important role in improving the surface activity and electrical conductivity of the material, which are fundamental aspects in the performance of gas sensors.

Furthermore, traces of the rutile ($TiO_2$) and carbonatite ($CaCO_3$) phases were identified. The presence of $TiO_2$ (a = b = 4.598 Å; c = 2.961 Å) is likely attributable to incomplete reaction of the titanium residue or phase segregation at elevated temperatures. The $CaCO_3$ phase (a = b = 5.071 Å; c = 16.411 Å) is hypothesized to have been formed as a result of the absorption of $CO_2$ gas from the atmosphere during the cooling process, which is a common phenomenon in calcium-based materials (Niu *et al*. 2022). The high-density value of $TiO_2$ (4.235 g/cm³) in comparison to $CaTiO_3$ and $CaCO_3$ (2.727 g/cm³) indicates the presence of denser and porous areas in the calcinated samples.

A modest augmentation in the lattice parameters b and c of $CaTiO_3$ between 900 °C and 1100 °C signifies the occurrence of thermal relaxation within the orthorhombic perovskite structure. This phenomenon suggests that an elevated calcination temperature enhances the diffusion kinetics of the atoms, thereby facilitating a more complete solid reaction and producing a more stable $CaTiO_3$ phase (Liu *et al*. 2026). The enhanced GoF and R-Bragg values further substantiate the conclusion that the crystal structure became more homogeneous, and the lattice strain diminished at elevated temperatures.

The presence of a secondary phase at 1100 °C suggests that total phase purity was not fully achieved. It is hypothesized that a longer calcination process or higher temperatures would be required to remove the entire impurity phase. However, the

refinement data demonstrate that a temperature of 1100 °C was sufficient to produce a well-structured, high-crystallized $CaTiO_3$ with a minimal number of impurity phases. The findings of this study are in accordance with those of earlier research conducted on the synthesis of perovskite titanate through solid-reaction methods.

The trend of increasing density obtained from the calculation demonstrates the densification behavior in accordance with calcination theory (Hsiang *et al*. 2023). It has been demonstrated that, at elevated temperatures, the density of $CaTiO_3$ integration exhibits relative stability, with a value of approximately 4.02 g/cm³. This observation suggests that the process of lattice solidification is more predominant than that of phase change. This structural stability is of paramount importance for dielectric and catalytic applications that demand high phase integrity at elevated operating temperatures.

## Morphological Characteristics of $CaTiO_3$

The surface morphology of calcined $CaTiO_3$ powder at 900 °C was analyzed using SEM, as illustrated in Fig. 3a. The SEM image indicates that the sample exhibited an irregular aggregate morphology, comprising fine primary particles with a grain size range of approximately ± 200 to 300 nm. This was measured by means of the ImageJ software. The particles appear to form loose lumps with a high number of pores between the grains. This indicates that the calcination process had not been completed at this temperature.

The surface of the material appears to be both rough and inhomogeneous, with the presence of residual precursor phases such as $CaCO_3$ and $Ca(OH)_2$. The existence of these two phases is in accordance with the results of Match! and Rietica analysis, which demonstrated that the reaction of solids between $CaCO_3$ and $TiO_2$ was not yet fully complete at a temperature of 900 °C. The failure of the reaction gave rise to the growth of grains that are suboptimal in size and the formation of porous structures and aggregates.

At this stage, the synthesis process was still in the initial phase of the formation of the nucleus (nucleation) of perovskite $CaTiO_3$. The thermal energy generated at 900 °C was not yet sufficient to promote the complete diffusion of $Ca^{2+}$ and $Ti^{4+}$ ions within the crystal lattice, with the result that most particles still took the form of partial precursors. This morphological feature has been observed to be a common characteristic in perovskite materials that have undergone calcination at temperatures below their optimal values. At these temperatures, the processes of nucleation and grain growth are just commencing but have not yet attained the stage of complete densification (Cafra *et al*. 2024).

The porous structure that was observed was capable of providing a large specific surface area, which is qualitatively beneficial for gas sensor applications, since it multiplies the number of active sites available for gas adsorption (Panigrahi *et al*. 2024; Sharma *et al.* 2024). However, the presence of incompletely decomposed phases of $Ca(OH)_2$ and $CaCO_3$ integration has been shown to reduce the stability of the crystal and increase the electrical resistance, thus hindering the performance of the sensor at this stage. Consequently, a sample of $CaTiO_3$ at 900 °C can be categorized as a transitional structure, indicating an early stage of perovskite phase formation before reaching crystalline maturity at higher temperatures, such as 1100 °C. This condition gives rise to a substantial surface area, yet concomitantly results in reduced conductivity, thus rendering this material suboptimal for utilization in VOC sensor applications. However, analysis of the morphology at 900 °C provides a significant indication of the early formation of the perovskite phase $CaTiO_3$, which is fundamental to enhanced crystallinity and sensor performance at higher calcination temperatures.

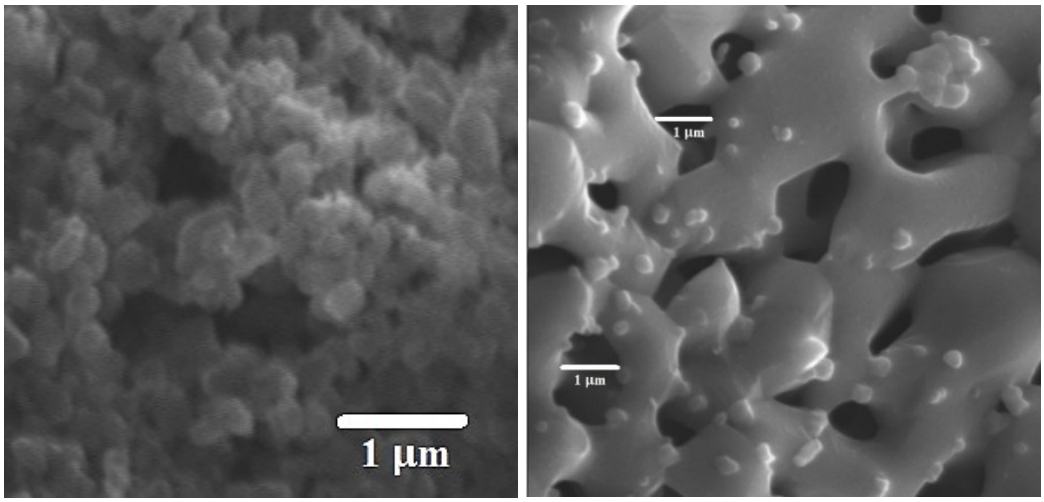


**Fig. 3.** Morphology of $CaTiO_3$ perovskite at (a) 900 °C and (b) 1100 °C calcination temperatures

**Table 3.** Results of the EDX of $CaTiO_3$ Perovskite at (a) 900 °C and (b) 1100 °C Calcination Temperatures

| Element | 900 °C | 1100 °C | | |
|---|---|---|---|---|
| | Wt (%) | At (%) | Wt (%) | At (%) |
| O | 28.10 | 35.02 | 42.56 | 66.56 |
| Ca | 27.47 | 21.08 | 3.57 | 2.23 |
| Ti | 34.02 | 26.17 | 59.73 | 31.21 |
| Si | 0.02 | 0.03 | - | - |
| Al | 0.07 | 0.09 | - | - |
| Mg | 0.17 | 0.21 | - | - |
| K | 0.19 | 0.25 | - | - |
| Na | 2.17 | 2.85 | - | - |
| Cl | 0.98 | 1.26 | - | - |

SEM imaging results at calcination temperature 1100 °C (Fig. 3b) demonstrated relatively homogeneous surface morphology with irregularly shaped granules. The grain size varied in the submicron range up to approximately 1.0 µm, with the presence of small pores scattered between the particle agglomerates. The porous structure is advantageous for gas sensor applications because it increases the effective surface area of the material and facilitates gas diffusion into the sensor layer.

The presence of fine pores and clear grain boundaries indicates that the calcination process at a temperature of 1100°C produces partial densification, in which grain growth had occurred but had not yet closed the porosity completely. These conditions are optimal for sensor materials, as they offer a balance between electrical conductivity and surface activity (Li and Xie 2023). The pores function as a diffusion pathway for VOCs, with the contact area between the grains playing a role in the mechanism of resistance change during the gas adsorption and desorption process.

At a calcination temperature of 1100 °C, the EDX spectrum showed that only Ca, Ti, and O elements were detected, in the absence of peaks of other elements (Table 3). This indicates that the calcination process at high temperatures led to the complete decomposition of intermediate compounds and evaporation of volatile components, resulting in a material with a more homogeneous composition and close to the theoretical

composition. These results are in accordance with a study carried out by Kurniawidi *et al.* (2025), which yielded $CaTiO_3$ from *Pinctada maxima* shell waste. The titanium element exhibited the highest mass percentage, accounting for 61.30% of the total, while its atomic percentage was 36.22%. O was present with a mass percentage of 34.30% and the highest atomic percentage of 60.68%, indicating its key role in the formation of oxides in the material.

The perovskite structures identified from the results of Rietica play an important role in the sensory activity of this material. The $Ti^{4+}$ cation at the B-site position has the potential to experience valence fluctuations when oxygen adsorption or reaction with gas molecules occurs. This phenomenon results in a change in the concentration of charge carriers (electrons) on the surface, which directly affects the value of the electrical resistance of the sensor. The oxygen vacuum formed during the calcination process has also been demonstrated to increase the material's ability to adsorb oxidative and reductive gases (Ramanavicius *et al.* 2022).

The integration of a stable crystal structure, as demonstrated by Rietica's refinement of the XRD data, and a homogeneous porous morphology, as observed from the SEM images, confirmed that the $CaTiO_3$ had favorable characteristics for gas sensing applications. It is clear that this structural feature was associated with improved sensing performance in oxide materials. The porous morphology provided an accessible surface area. This surface area may facilitate gas–surface interaction (Verma *et al.* 2025). Enhanced interaction is often beneficial for adsorption processes (Passi and Pal 2021). Phase stability is another important factor. Stable phases are generally considered beneficial for maintaining signal consistency. This aspect is particularly relevant during repeated operation at elevated temperatures. Previous studies by Lin *et al.* (2019) have shown that the interface between $CaTiO_3$ and $TiO_2$ creates a heterojunction. This junction affects how the charge moves and how the resistance changes when the material is exposed to gas. The presence of this secondary phase will definitely affect how the sensor works. The structure and shape of $CaTiO_3$ samples heated to 1100 °C indicate that this material is a strong candidate for use in VOC gas detection sensors. However, more research is needed to fully understand its function as a sensor and the way charges pass through it.

From this study, the $CaTiO_3$ material synthesized from the shell has the advantage of the porous structure formed naturally from the biogenic morphology of the precursor, resulting in a surface area and pore distribution that supports the diffusion and adsorption of VOC molecules to the active surface. This porous character is important in increasing the number of gas–surface interaction sites and accelerating sensor response kinetics. On the other hand, the study of lignocellulose biomass and its structural polymers (cellulose, hemicellulose and lignin) carried out by Isinkaralar (2025) also demonstrated a porous hierarchical structure and high surface area that supports adsorption as well as functionalization of chemistry for (bio)sensing applications. Thus, both shell-based and lignocellulose $CaTiO_3$ take advantage of the porosity character as a key factor in increased sensitivity. However, $CaTiO_3$ integration plays more of a role as a stable semiconductor transducer. Lignocellulose also excels as an adsorbent matrix and a continuous surface modification platform.

## CONCLUSIONS

1. This study demonstrated that an increase in calcination temperature exerted a significant influence on the formation and stability of $CaTiO_3$ phase, which was synthesized from thick clam shell biomineral sources. It was demonstrated that, at elevated temperatures, the perovskite phase adopted an orthorhombic structure, thus becoming the predominant phase and exhibiting enhanced crystallinity. This assertion was substantiated by rigorous XRD analysis and Rietveld refinement, which consistently yielded superior fit parameters. This finding suggests that the solid-state reaction process was relatively complete and that there was an increase in structural regularity.
2. Scanning electron microscope (SEM) analysis revealed that the grains exhibited enhanced integration, accompanied by an augmentation in connectivity between them. This progression was attributed to the elevated calcination temperature, which prompted the evolution of the grains. This microstructural modification qualitatively enhanced the efficiency of diffusion and densification processes, thereby contributing to an improvement in the overall material properties.
3. The natural porosity of the Tebalan seashells-based $CaTiO_3$ and the hierarchical structure of lignocellulose both contribute to improved VOC interaction and adsorption, but they offer different mechanisms and roles in sensor systems, potentially combining to produce more sensitive and sustainable detection devices.

## ACKNOWLEDGMENTS

The present research was funded by the Ministry of Education, Culture, Research, and Technology budget for the 2025 fiscal year. This funding was granted based on the Fundamental Research Scheme, as outlined in Decree Number 0419/C3/DT.05.00/2025. In addition, the laboratory staff should be commended for their technical assistance during the pharmaceutical laboratory activities of Nahdlatul Ulama Sunan Giri University. Expressions of gratitude are also directed towards the Energy and Environment Laboratory of the Sepuluh Nopember Institute of Technology, whose efforts facilitated the analysis of XRD and SEM.

## REFERENCES CITED

Adamová, T., Hradecký, J., and Pánek, M. (2020). "Volatile organic compounds (VOCs) from wood and wood-based panels: Methods for evaluation, potential health risks, and mitigation," *Polymers* 12(10), article 2289. https://doi.org/10.3390/polym12102289

Cafra, B., Alberti, A., Calogero, G., Deretzis, I., Landi, A., Pagano, D., Sanzaro, S., and La Magna, A. (2024). "Mechanism of grain densification in nano- and poly-crystalline Cu films and its impact in advanced metallization processes," *Crystals* 14(2), article 125. https://doi.org/10.3390/cryst14020125

David, E., and Niculescu, V.-C. (2021). "Volatile organic compounds (VOCs) as environmental pollutants: Occurrence and mitigation using nanomaterials,"

*International Journal of Environmental Research and Public Health* 18(24), article 13147. https://doi.org/10.3390/ijerph182413147

Dehghani, M. H., Bashardoust, P., Zirrahi, F., Ajami, B., Ghalhari, M. R., Noruzzade, E., Sheikhi, S., Mubarak, N. M., Karri, R. R., and Ravindran, G. (2024). "Environmental and health effects due to volatile organic compounds," in: *Health Effects of Indoor Air Pollution*, pp. 191-221. https://doi.org/10.1016/B978-0-323-91154-0.00012-1

Hill, C., Altgen, M., and Rautkari, L. (2021). "Thermal modification of wood—A review: Chemical changes and hygroscopicity," *Journal of Materials Science* 56(11), 6581-6614. https://doi.org/10.1007/s10853-020-05722-z

Hossain, M. S., and Takshi, A. (2021). "Perovskite-based sensing scheme for detecting volatile organic compounds (VOCs) at room temperature," *MRS Advances* 6(26), 645-649. https://doi.org/10.1557/s43580-021-00080-7

Hsiang, H.-I., Yang, Y.-H., Huang, C.-Y., and Yang, K. (2023). "Effects of calcination on the dielectric properties and insulation resistance of $Ba_{0.95}Ca_{0.05}TiO_3$ ceramics sintered in a reducing atmosphere," *Journal of Alloys and Compounds* 960, article 170919. https://doi.org/10.1016/j.jallcom.2023.170919

Li, W., and Xie, K. (2023). "Porous single crystals at the macroscale: From growth to application," *Accounts of Chemical Research* 56(3), 374-384. https://doi.org/10.1021/acs.accounts.2c00777

Liu, Q., Li, Y., Su, Y., Fan, Y., Hu, F., Li, C., Tian, L., Luo, Y., Cao, B., and Xu, L. (2026). "Challenges and strategic approaches to constructing the full life cycle value chain of layered cathode materials for sodium-ion batteries," *Nano Research* 5, article e9120177. https://doi.org/10.1007/s12274-025-9120177

Niu, Y.-Q., Liu, J.-H., Aymonier, C., Fermani, S., Kralj, D., Falini, G., and Zhou, C.-H. (2022). "Calcium carbonate: Controlled synthesis, surface functionalization, and nanostructured materials," *Chemical Society Reviews* 51(18), 7883-7943. https://doi.org/10.1039/D2CS00262H

Panigrahi, P. K., Chandu, B., and Puvvada, N. (2024). "Recent advances in nanostructured materials for application as gas sensors," *ACS Omega* 9(1), article e06533. https://doi.org/10.1021/acsomega.3c06533

Ray, A., and Basu, T. (2023). "Perovskite metal oxide-based composite materials: Potential candidates for electronics and optoelectronics," in: *Perovskite Metal Oxides*, Elsevier, pp. 203-229. https://doi.org/10.1016/B978-0-323-99529-0.00024-2

Rohmah, R., Yuwita, P. E., Pangestu, P. D., and Vibianto, E. D. A. (2024). "Potential of Tebalan shells from Tuban Beach as active material in perovskite solar cells," *Jurnal Pendidikan Fisika dan Teknologi* 10(2), 437-444. https://doi.org/10.29303/jpft.v10i2.546

Rong, Y., Pan, C., Song, K., Nam, J. C., Wu, F., You, Z., Hao, Z., Li, J., and Zhang, Z. (2023). "Bamboo-derived hydrophobic porous graphitized carbon for adsorption of volatile organic compounds," *Chemical Engineering Journal* 461, article 141979. https://doi.org/10.1016/j.cej.2023.141979

Sharma, A., Eadi, S. B., Noothalapati, H., Otyepka, M., Lee, H.-D., and Jayaramulu, K. (2024). "Porous materials as effective chemiresistive gas sensors," *Chemical Society Reviews* 53(5), 2530-2577. https://doi.org/10.1039/D3CS00849K

Singh, P., Bansal, N. K., Dey, S., Singh, R., and Singh, T. (2024). "Recent progress on perovskite materials for VOC gas sensing," *Langmuir* 40(42), 21931-21956. https://doi.org/10.1021/acs.langmuir.4c02089

Tan, W., Hu, P., Feng, T., Zhao, S., Wang, S., Song, H., Qi, Z., and Li, W. (2025). "Effects of Cu substituting Mo in $Sr_2Fe_{1.5}Mo_{0.5}O_{6-\delta}$ symmetrical electrodes for $CO_2$ electrolysis in solid oxide electrolysis cells," *Nanomaterials* 15(8), article 585. https://doi.org/10.3390/nano15080585

Toso, S., Baranov, D., Filippi, U., Giannini, C., and Manna, L. (2023). "Collective diffraction effects in perovskite nanocrystal superlattices," *Accounts of Chemical Research* 56(1), 66-76. https://doi.org/10.1021/acs.accounts.2c00613

Wang, Z., Lin, R., Huo, Y., Li, H., and Wang, L. (2022). "Formation, detection, and function of oxygen vacancy in metal oxides for solar energy conversion," *Advanced Functional Materials* 32(7), article 2109503. https://doi.org/10.1002/adfm.202109503

Wawrzyniak, J. (2023). "Advancements in improving selectivity of metal oxide semiconductor gas sensors opening new perspectives for their application in food industry," *Sensors* 23(23), article 9548. https://doi.org/10.3390/s23239548

Wu, H., Meng, F., Gong, X., Tao, W., Zhao, L., Wang, T., Liu, F., Yan, X., Sun, P., and Lu, G. (2023). "A solution to boost acetone sensing performance of perovskite oxides chemiresistors: In-situ derived p–p heterostructures," *Sensors and Actuators B: Chemical* 378, article 133092. https://doi.org/10.1016/j.snb.2023.133092

Zhang, J., Shao, J., Zhang, X., Jiang, H., Zhang, S., Zhang, S., Yang, H., and Chen, H. (2024). "Molecular simulation of different VOCs adsorption on nitrogen-doped biochar," *Fuel* 372, article 132127. https://doi.org/10.1016/j.fuel.2024.132127

Zhang, W., Li, G., Yin, H., Zhao, K., Zhao, H., and An, T. (2022). "Adsorption and desorption mechanism of aromatic VOCs onto porous carbon adsorbents for emission control and resource recovery: Recent progress and challenges," *Environmental Science: Nano* 9(1), 81-104. https://doi.org/10.1039/D1EN00944J

Zhou, X., Zhou, X., Wang, C., and Zhou, H. (2023). "Environmental and human health impacts of volatile organic compounds: A perspective review," *Chemosphere* 313, article 137489. https://doi.org/10.1016/j.chemosphere.2022.137489

Zhu, S., Zhu, J., Ye, S., Yang, K., Li, M., Wang, H., and He, J. (2023). "High-entropy rare earth titanates with low thermal conductivity designed by lattice distortion," *Journal of the American Ceramic Society* 106(10), 6279-6291. https://doi.org/10.1111/jace.19233

Zouari, M., Marrot, L., and DeVallance, D. B. (2023). "Evaluation of properties and formaldehyde removal efficiency of biocarbon prepared at variable pyrolytic temperatures," *Frontiers in Environmental Science* 11, article 1252926. https://doi.org/10.3389/fenvs.2023.1252926

Article submitted: October 12, 2025; Peer review completed: February 7, 2026; Revised version received and accepted: February 21, 2026; Published: February 27, 2026.
DOI: 10.15376/biores.21.2.3609-3621